Hindawi
Journal of Chemistry
Volume 2024, Article ID 4244579, 14 pages
https://doi.org/10.1155/2024/4244579

Research Article

Mechanistics of pH-Dependent Sulfmyoglobin Formation: Spin Control and His64 Proton Relay

Angel D. Rodriguez-Mackenzie,[1] Lysmarie Santos-Velazquez,[1] Héctor D. Arbelo-Lopez,[1] Troy Wymore ,[2] and Juan Lopez-Garriga [1,3]

[1]*Department of Chemistry, University of Puerto Rico Mayaguez Campus, Mayaguez, PR 00680, USA*
[2]*Laufer Center Stony Brook University, Stony Brook, NY 117945252, USA*
[3]*Industrial Biotechnology Program, University of Puerto Rico at Mayaguez Campus, Mayaguez, PR 00681, USA*

Correspondence should be addressed to Troy Wymore; troy.wymore@stonybrook.edu and Juan Lopez-Garriga; juan.lopez16@upr.edu

Received 21 November 2022; Revised 18 January 2024; Accepted 2 February 2024; Published 21 February 2024

Academic Editor: Jose Corchado

The chemistry of hydrogen sulfide (H_2S) has been directed towards physiologically relevant hemeproteins, including myoglobin, hemoglobin, and other similar proteins. Despite substantial efforts, there remains a need to elucidate the mechanism and identify the species involved in the reaction between oxy-hemeproteins and H_2S. Here, we summarize both our experimental data and computational modeling results revealing the mechanisms by which sulfmyoglobin (sulfMb) and sulfhemoglobin (sulfHb) are formed. Our experimental data at pH 7.4 reveal differences in intensity between sulfMb and sulfHb chromophores in the 620 nm charge transfer region. This behavior could be attributed to the incomplete reaction of tetrameric oxy-Hb with H_2S, where not all heme groups form sulfheme. The data also show that, for the reaction of oxy-myoglobin (oxy-Mb) and H_2S, the 622 nm charge transfer band increases in intensity from a pH of 6.6 to 5.0. This increase is attributed to the presence of the heme pocket distal $His64_{\varepsilon\delta}$, which is positively charged, resulting in an elevated yield of sulfMb formation compared to the mono-protonated tautomer, $His64\varepsilon$. Computational hybrid QM/MM methods support the conclusion, indicating that oxy-Mb $His64_{\varepsilon\delta}$ (pH 5.0) reacts with H_2S in the triplet state, favored by −31.0 kcal/mol over the singlet $His64\varepsilon$ (pH 6.6) species. The phenomenon is facilitated by a hydrogen bonding network within the heme pocket, between $His64_{\varepsilon\delta}$, heme $Fe(II)O_2$, and H_2S. The results establish an energetically favored quantitative mechanism to produce sulfMb (−69.1 kcal/mol) from the reactions of oxy-Mb and H_2S. Curiously, the mechanism between met-aquo Mb, H_2O_2, and H_2S shows similar reaction pathways and leads to sulfheme formation (−135.3 kcal/mol). The energetic barrier towards intermediate Cpd-0 is the limiting step in sulfheme formation for both systems. Both mechanisms show that the thiyl radical, $HS^{\bullet}$, is the species attacking the β-β double bond of heme pyrrole B, leading to the sulfheme structure.

1. Introduction

Hydrogen sulfide (H_2S) is a gas endogenously produced in mammalian tissues and organs by the enzymes cystathionine β-synthase (CBS), cystathionine ɣ-lyase (CSE), D-amino acid oxidase (DAO), and indirectly by 3-mercaptopyruvate sulfurtransferase (3-MST) [1–4]. H_2S concentrations and enzyme distribution in tissues are correlated with physiological function [1–4] due to the highly lipophilic nature of H_2S that facilitates easy penetration into the cell by simple diffusion [5]. H_2S plasma values can vary between 50 μM and 150 μM and are associated with several conditions, including the fibrosis phenomenon [6]. In addition, SARS-CoV-2 survivors show serum H_2S levels that are higher (≥150 μM) than those of nonsurvivors [7, 8]. Thus, the production of H_2S has been suggested to act as a defense mechanism against COVID-19 [8–10]. Overexpressed CSE in the pancreas increases H_2S levels, inducing the pathogenesis of diabetes in rats [11]. In contrast, a reduction in the enzymatic activity of CSE promoted hypertension in rats and

women with preeclampsia [12, 13]. Reduced H_2S levels are also related to Parkinson's, Alzheimer's, and atherosclerosis [14, 15]. Furthermore, H_2S has been correlated with chronic diseases [16, 17], inflammation [18, 19], oxidative stress [20–25], oral diseases [26], glaucoma [27], subarachnoid hemorrhage [28], infertile men [29], arterial oxygen saturation [30], and skin diseases [31].

Human exposure to exogenous concentrations of H_2S can trigger sulfhemoglobinemia-induced cyanosis, a bluish skin color associated with the lack of oxygen [13, 32–41]. In addition, excessive amounts of drugs such as acetanilide, metoclopramide, phenacetin, dapsone, and sulfanilamide-containing medications produce the same physiological condition [32]. The phenomena have been observed in the newborn [33], gamma rays' irradiation [34, 35], cancer, neurodegenerative diseases [36], and dimethyl sulfide (DMSO) dermal applications [37].

Sulfhemoglobinemia [38–41] is associated with hemoglobin and myoglobin, presenting an oxygen reduction affinity of 135 and 2,500 times upon sulfhemoglobin (sulfHb) and sulfmyoglobin (sulfMb) formation, respectively [42]. Normal levels of physiological sulfhemoglobin are below 0.037 g/dL, whereas 0.5 g/dL in the blood is enough to present cyanosis symptoms [13, 43, 44]. A consensus on the relationship between pH, oxy-hemoglobin (oxy-Hb), oxy-myoglobin (oxy-Mb), and hydrogen sulfide to produce sulfHb and sulfMb has still not been reached. Experimentally, the reaction between H_2S and met-aquo-Hb[Fe(III)] or met-aquo-Mb [Fe(III)] in the presence of H_2O_2 and oxy-Hb [Fe(II)] and oxy-Mb[Fe(II)] under an O_2 environment generates sulfHb and sulfMb (reactions (1a) and (1b)), respectively [45–47].

$$\text{met} - \text{aquo} - \text{Mb}\,[\text{Fe}\,(\text{III})] + H_2O_2 + H_2S \longrightarrow \text{sulfMb} + 2\,H_2O, \tag{1a}$$

$$\text{oxy-Mb}\,[\text{Fe}\,(\text{II})] + O_2 + 2H_2S \longrightarrow \text{sulfMb} + 2\,H_2O + SH^{-}. \tag{1b}$$

Radioactive sulfide species demonstrated that a single sulfur atom is incorporated into the heme structure per mol of Mb to form sulfMb [47]. The insertion resulted in a covalent heme modification by the specific incorporation of the sulfur ring across the β-β double bond of heme pyrrole B, Figure 1. X-ray [48] and NMR [49] spectroscopy have supported the structural assignment. The chromophore shows a characteristic optical band in the 620 nm region. Slight displacements of this band depend on the isomer and ligation states [42, 46, 49–52]. The absorption region is characterized by a π to dπ (dyz, dxz) charge transfer transition associated with the sulfur ring attached to the pyrrole B and the heme iron [53].

Interestingly, an inverse relationship between increased sulfMb formation and a pH decrease has been shown in reaction (1a). Thus, it has been suggested that H2S, rather than its anion (HS-), is the reactive sulfur species in the sulfheme reaction mechanism [54, 55]. Furthermore, several hemeproteins were evaluated for their reaction with H_2O_2 in the presence of H_2S. The data revealed that the formation of the sulfheme derivative requires the presence of the His64 residue in the distal heme site [56]. All other amino acids tested at this position generate the classical heme-ferryl compound I radical [Fe(IV)=$O^{+\bullet}$, Cpd-I] and heme ferryl compound II [hemeFe(IV)=O, Cpd-II]. Two different pathways have been proposed [46, 47, 55, 57, 58] to explain sulfheme formation. In one scheme, Berzofsky et al. [46, 47] suggested that the hydrosulfide ion (HS^{-}) may be the initial reactant species because ~70% of H_2S dissociates to HS^{-} (pKa of 7.40) at physiological pH. Yet, experiments indicate that sulfMb presence decreases by 250-fold at basic pH values, at which the predominant species is HS^{-} [55], suggesting that this is not the leading reactive species. On the other hand, Nicholls et al. [57] proposed that sulfMb can be formed stoichiometrically upon the reaction of Cpd-II with a thiyl radical, $HS^{\bullet}$, and that a mixture of ferric sulfMb and small quantities of ferrous sulfMb were generated as final products [57, 58].

QM/MM calculations showed that a concerted interaction among the heme, distal His64, H_2O_2, and H_2S led to the formation of the thiyl radical, $HS^{\bullet}$, necessary for sulfheme formation [53, 56, 59]. The calculations suggest a sulfheme mechanism initiated by hydrogen bonding interactions among heme Fe(III)–H_2O_2, His64, and H_2S. Figure 1S (supplementary information) depicts a favorable formation of the intermediate Cpd-0 [Fe(III)OOH] that reacts with hydrogen sulfide to produce, upon homolytic cleavage of both Cpd-0 and an S-H bond, a favorable heme ferryl compound II and a thiyl radical, $HS^{\bullet}$. The reaction is subsequently followed by a reaction between hemeFe(IV) =O and the $HS^{\bullet}$ radical, leading to a −135.3 kcal/mol potential energy decrease which correlates with the sulfMb kinetics ($2.5 \pm 0.1 \times 10^6\ M^{-1}s^{-1}$) and stability. Although the mechanism to generate the heme ferryl compound II and a thiyl radical, $HS^{\bullet}$, is different from the model proposed by Nicholls [57], the calculated energetic data indeed supported their hypothesis of the reaction between hemeFe(IV)=O and the $HS^{\bullet}$ to produce sulfheme. Furthermore, contrary to the classical peroxidative reaction of heme proteins with H_2O_2 [60, 61],the absence of the heme Cpd-I radical [Fe(IV)=$O^{+\bullet}$] in sulfheme formation through reaction (1a) [53, 59] supports the antioxidant role of hydrogen sulfide [18–25].

Early results show that the reaction between oxy-Mb and hydrogen sulfide, in the presence of fully protonated $His64_{\varepsilon\delta}$, promotes an energetically favorable path (−31.0 kcal/mol) from a heme ligand singlet to a triplet state that stabilizes the heme compound-III [Fe(III)O-O^{-}, Cpd-III], Scheme 1 [62].

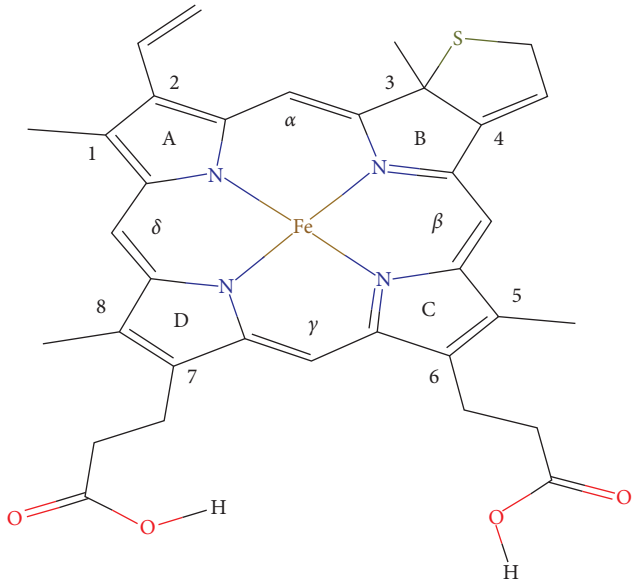

Figure 1: Sulfheme chromophore.

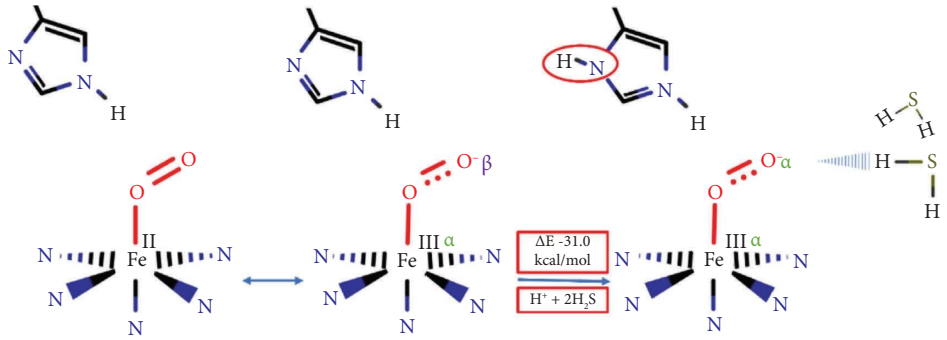

Scheme 1: Stabilization of heme compound III by hydrogen sulfide.

Moreover, a synchronized higher energy process accompanies the transition from Cpd-III and H_2S to heme compound 0 [Fe(III)-OOH, Cpd-0]. Thus, Scheme 2 presents a 23.3 kcal/mol barrier coupled with the homolytic cleavage of an S-H bond, following the favorable (−11.2 kcal/mol) formation of transient Cpd-0 and thiyl radical ($HS^{\bullet}$) [62]. However, despite this knowledge, the mechanism for sulfheme formation (reaction (1b)), intermediate structure, pH dependence, and the relation to its electronic charge transfer 620 nm band region have remained unresolved. The report presented here builds upon earlier research [62], examining the influence of pH on the populations of heme-ligand triplets and singlets, as well as the His64 proton relay within the heme pocket. The results show that oxy-Mb interacting with H_2S to produce the 5-member ring met-aquo-sulfMb (SC) from the Cpd-0 intermediate is energetically favorable by ΔE −69.1 kcal/mol. Experimental results support the pH-related behavior and how the triplet-to-singlet transition affects the 622 nm absorption intensity and the population of sulfheme.

2. Materials and Methods

2.1. Experimental Sulfmyoglobin (sulfMb) and Sulfhemoglobin (sulfHb) Formation. Myoglobin (Mb) from equine skeletal muscle and human hemoglobin obtained from Sigma-Aldrich were used without further purification. The hemeproteins deoxy-Mb (Soret (435 nm) and Q (560 nm)) and deoxy-Hb (Soret (430 nm) and Q (555 nm)) species [hemeFe(II)], in HEPES buffer 0.05M pH = 7.4, were obtained upon anaerobic reduction of the met-aquo-hemeproteins [hemeFe(III)] with sodium dithionite. All solutions were degassed and then purged with $N_{2(g)}$ for three cycles of 15 minutes each. At pH 7.4, the Mb : $Na_2S_2O_4$ and Hb : $Na_2S_2O_4$ molar ratio was 1 : 2. At pH 5.0 and 6.6, sperm whale deoxy-myoglobin was prepared in phosphate and succinic acid buffer solution with an Mb : $Na_2S_2O_4$ molar ratio of 1 : 8 [42, 45–47]. All samples were prepared under anaerobic conditions. The oxy-Mb and oxy-Hb derivatives were prepared by saturating deoxy-Mb and deoxy-Hb solutions with ultrapure dioxygen gas for 30 minutes and 10

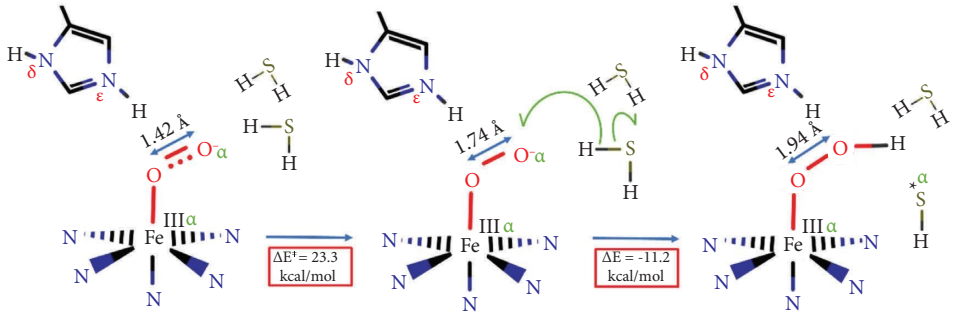

Scheme 2: Formation of heme compound 0 and thiyl radical. Notice that His64$_{\varepsilon\delta}$ has the delta and epsilon nitrogens (Nε and Nδ) identified.

psi. They showed the characteristics of the electronic transitions at Soret (418 nm) and Q (542 nm and 580 nm) and Soret (415 nm) and Q (541 nm and 577 nm), respectively, [42, 45–47, 63, 64].

Hydrogen sulfide solutions were prepared from sodium sulfide salts (Na_2S) in the same buffer solution as the hemeproteins. Hydrogen sulfide stock solution (83 mM) was prepared in an amber vial with 0.020 g of $Na_2S{\cdot}9\ H_2O$ salt (Alfa Aesar) previously purged with nitrogen and 1.0 mL of HEPES 0.0500M buffer at a pH of 7.4. In HEPES buffer at pH 7.4, there is an equilibrium between 80% SH^- and 20% H_2S, while in phosphate and succinic acid, at pH 5.0 and 6.6, the predominant species is H_2S. At pH 7.4, sulfmyoglobin (sulfMb) and sulfhemoglobin (sulfHb) derivatives in the HEPES buffer were prepared by the reaction between oxy-Mb (55 μM) and oxy-Hb (55 μM) solutions with hydrogen sulfide (H_2S) solution in a molar ratio of 1 : 3 (oxy-hemeprotein H_2S). The hydrogen sulfide concentration was 165 μM. The scenario allowed us to understand the differences between the monomeric sulfMb and the tetrameric sulfHb and the charge transfer band in the 620 nm region, characteristic of the sulfheme formation [42, 45–47, 53, 59, 65]. Sulfmyoglobin at pH 5.0 and 6.6 was prepared from sperm whale oxy-myoglobin in phosphate and succinic acid buffer solution by mixing the oxy-Mb solution with H_2S solution at the same pH in a 1 : 100 molar ratio, oxy-Mb : H_2S. UV-Vis spectral data were collected on a SHIMADZU 2600 UV-Vis with a temperature controller set at a constant temperature of 25°C.

2.2. Theoretical Methods for Sulfmyoglobin Formation. The crystal structure coordinates of Equus caballus myoglobin 2VLY [66] were obtained from the RCSB protein data bank, which has a resolution of 1.6 Å. Models were constructed using CHARMM version 40b [67], describing the protein and solvent with CHARMM36 force field with CMAP correction [68] and the TIP3P water model [69], respectively. The description of the heme moiety used a CHARMM-modified force field [70]. The active site residue His64 was modeled in acidic pH with N_ε and N_δ protonated. All other residues were modeled in their canonical protonation states. Potassium and chloride ions were added to the solvated system at a concentration of 0.15 M with the Monte Carlo simulation method, resulting in a model size of 71 Å3 composed of 33,330 atoms. The models were all geometry optimized for 1000 steps using the steepest decent algorithm. The models were then simulated for 500 picoseconds (ps) at 300K, restraining the heavy atoms of the protein and heme with a harmonic force constant of 5 and 50 kcal/(mol Å), respectively. Finally, the SHAKE algorithm [71] was used to constrain all bonds to hydrogen to enable 2 fs time steps. These simulations' primary objective was equilibrating the surrounding water molecules and those near the active site. Figure 2S (Supporting Information) shows the integrated model used for the calculations.

2.3. Refinement of Models Using PM6/MM Simulations. Hybrid QM/MM simulations were performed with pDynamo version 1.9 [72]. Electrostatic and Van der Waals interactions had an inner cutoff distance of 8 Å and an outer cutoff distance of 14 Å. The QM region consisted of the entire heme group, propionate and vinyl groups, residue His93, and the O_2 ligand for 92 atoms in the singlet state [73]. The models were geometry optimized with the SD algorithm for 1000 steps. The atomic velocities were scaled every 50 steps (1 fs time step) to simulate the models from 10 K to 300 over 3 ps. The models were then simulated for another 10 ps at 300 K. The final snapshot was used to model the interactions of H_2O and H_2S molecules with oxy-Mb using the Density Functional Theory (DFT) method. Visualization of the structures and analysis were performed with the VMD program [74].

2.4. DFT/MM Calculations Sulfmyoglobin Formation. Hybrid DFT/MM simulations were performed to unravel the sulfmyoglobin formation mechanism from the oxy-Mb reaction with H_2S with pDynamo interfaced with the ORCA program version 4.1 [75]. The models were truncated from the previous cubic model, deleting all water molecules and ions outside a 30 Å sphere centered on the Fe atom. All protein residues, water molecules, and ions containing an atom within 22 Å of the Fe atom were unrestrained; all others were fixed in position. Two water molecules that always entered and remained in the active site His64$_{\varepsilon\delta}$ model during the PM6/MM simulations were replaced by H_2S molecules. The QM region consisted of the entire heme moiety, including propionate and vinyl groups, His64, His93, Val68, Leu29, Phe43, O_2, H_2S, and H_2O molecules. A total of 146 atoms were included in the MbHis64$_{\varepsilon\delta}$

calculation. The hydrogen link atom approach was used to define the QM/MM boundary. Before substituting the H_2O molecule(s) with H_2S replacement, the models were geometry optimized for 300 steps using the SD algorithm and then by the conjugate gradient algorithm for 700 steps using the unrestricted DFT functional BP86 [76–78] with the D3 dispersion correction [79, 80]. The basis set was Ahlrichs triple-zeta with polarization TZVP and the Def2/J [81–83] resolution of identity approximation (RI). A Stuttgart-Dresden-Bonn relativistic effective core potential (ECP) was used for the iron atom [84, 85]. The calculations use the libint2 library to compute 2-electron integrals as specified by ORCA [86]. A total of thirty models were constructed by alternating multiplicity, H_2S/H_2O molecule positions, and availability of the Fe atom. After the replacement of H_2O by H_2S molecules, the models were geometry optimized for another 300 steps using the SD algorithm.

The energetic profile of Cpd-0 formation was calculated using the O=O bond length as the reaction coordinate over 20 windows in increments of 0.05 Å. Each window was geometry optimized with 50 steps of the SD algorithm using a force constant of 400 kcal/(mol Å) on the reaction coordinate. An accurate energy profile and the potential energy of the structures along the reaction coordinates were obtained using the BP86/MM method. It was calculated with the unrestricted hybrid functional B3LYP [87, 88] with TZVP and Def2/J auxiliary basis sets and RIJCOSX approximation for the Coulomb and Hartree–Fock (HF) exchange integrals. The functional was modified to have an HF exchange of 13%, providing more accurate energy values for iron-containing systems [89, 90]. The quasi-restricted orbitals obtained from the DFT-defined region were used to explore the effects of spin contamination with a restricted open-shell Kohn–Sham (ROKS) description of the QM region. When performing single energy points on ROKS, the RIJONX approximation for the Coulomb integrals was used. Spin density was calculated using the ORCA plot interactive suite of the ORCA 4.0.1 software. The conformations of interest were those at the local and global minima of the reaction coordinates. Corroboration of the triplet spin state system was performed by CASSCF using the TZVP basis set, Def2/JK auxiliary basis set, and RIJCOSX approximation. Our initial guess was generated using the resulting quasi-restricted orbitals (QROs) from our previous ROKS calculations. The active space consisted of iron's 3d orbitals and six 2p orbitals of O_2, resulting in 11 orbitals and 14 electrons [91].

3. Results and Discussion

3.1. Insight of pH-Dependent Sulfmyoglobin Formation. The pH dependence is crucial in deciding the histidine amino acid tautomeric population and its role in protein function [92–94]. For example, myoglobin, at neutral pH, $His64_{\varepsilon}$ (HisE7), is predominantly mono-protonated on its nitrogen (N_{ε}), and its swinging motion opens and closes the heme pocket to ligand migration [95–97]. Thus, the heme-O_2-$His64_{\varepsilon}$ hydrogen bond interaction is thermodynamically favorable. On the other hand, the sulfMb species, sulfur-derived heme, requires the proper orientation of the His64 residue in the distal heme site [56]. Moreover, in the case of reaction (1a), an inverse relationship exists between an increased production yield and a decreased pH [54, 55]. Figure 2 displays the visible spectra illustrating the time-dependent sulfMb formation from the interaction of oxy-Mb with H_2S (reaction (1b)) under conditions of $His64_{\varepsilon}$ (pH 6.60) and $His64_{\varepsilon\delta}$ (pH 5.00). The consumption of H_2S by oxy-Mb results in a reduction in intensity of the electronic transitions at 543 nm and 580 nm. In contrast, the charge transfer band at 622 nm increases as the sulfMb population rises, in agreement with the literature [42, 45–47, 53].

A comparison between Figures 2(a) and 2(b) (pH 5.0) and Figures 2(c) and 2(d) (pH 6.6) shows that $His64_{\varepsilon\delta}$ drastically promotes sulfMb formation relative to the $His64_{\varepsilon}$ tautomer. At a more acidic pH, the 622 nm band increases in intensity, reaching its maximum absorbance from dark blue to bright blue in 30 minutes (Figure 2(b)), while the process at the higher pH takes 350 minutes (Figure 2(d)). The intensity increase reaches its maximum absorbance approximately ten-fold faster at lower than higher pH. Likewise, the transitions at 543 nm and 580 nm exhibit distinct behaviors at various pH levels, as evidenced by the alterations in red-to-orange color intensity (Figures 2(c) and 2(d)). Within this pH window, the probability of full protonation of distal His64 increases with more acidic environments, further enabling proton exchange within the heme distal cavity.

Early work [62], conducted at a millisecond scale using stopped-flow spectrophotometry, revealed that, at the more acidic pH of 5.0 during the reaction of oxy-Mb with H_2S, there is a transition of the Soret band from 414 nm to 416 nm, reaching a maximum absorbance value at 100 ms. The 2 nm red shift was suggested to be caused by the presence of heme Cpd-0 [Fe(III)OOH]. Hence, the findings indicate that protonation of the delta nitrogen of $His64_{\varepsilon\delta}$ (as defined in Scheme 2) enables the migration of the epsilon-located hydrogen, thereby facilitating reaction (1b) and augmenting the intensity of the 622 nm charge transfer transition. The stronger hydrogen bond between the nitrogen epsilon-located hydrogen and compound III dissipates emerging charged groups near the active site, facilitating Compound I formation, as discussed in the next section.

3.2. Insight into Sulfmyoglobin Formation Mechanism. The visible spectroscopic data between oxy-Mb and H_2S reactions were supported using two distinct models: (i) neutral (with $His64_{\varepsilon}$, pH 6.6) and (ii) positively charged histidine ($His64_{\varepsilon\delta}$, pH 5.0). Oxy-Mb with the $His64_{\varepsilon}$ tautomer and H_2S favored the open shell singlet biradical state over the triplet state by approximately 7.0 kcal/mol. In contrast, oxy-Mb $His64_{\varepsilon\delta}$ interaction with H_2S reveals that the triplet state is favored by 31.0 kcal/mol over the singlet biradical state (Scheme 1). In this paramagnetic triplet state, an unpaired electron occupies the central Fe d_{XZ} orbital, while the second unpaired electron is shared between the oxygen atoms bonded to heme. This electronic configuration is consistent with the heme compound III [Fe(III)O-$O^{\bullet-}$, Cpd-III] also known as superoxy-Mbor the Weiss configuration [62] shown

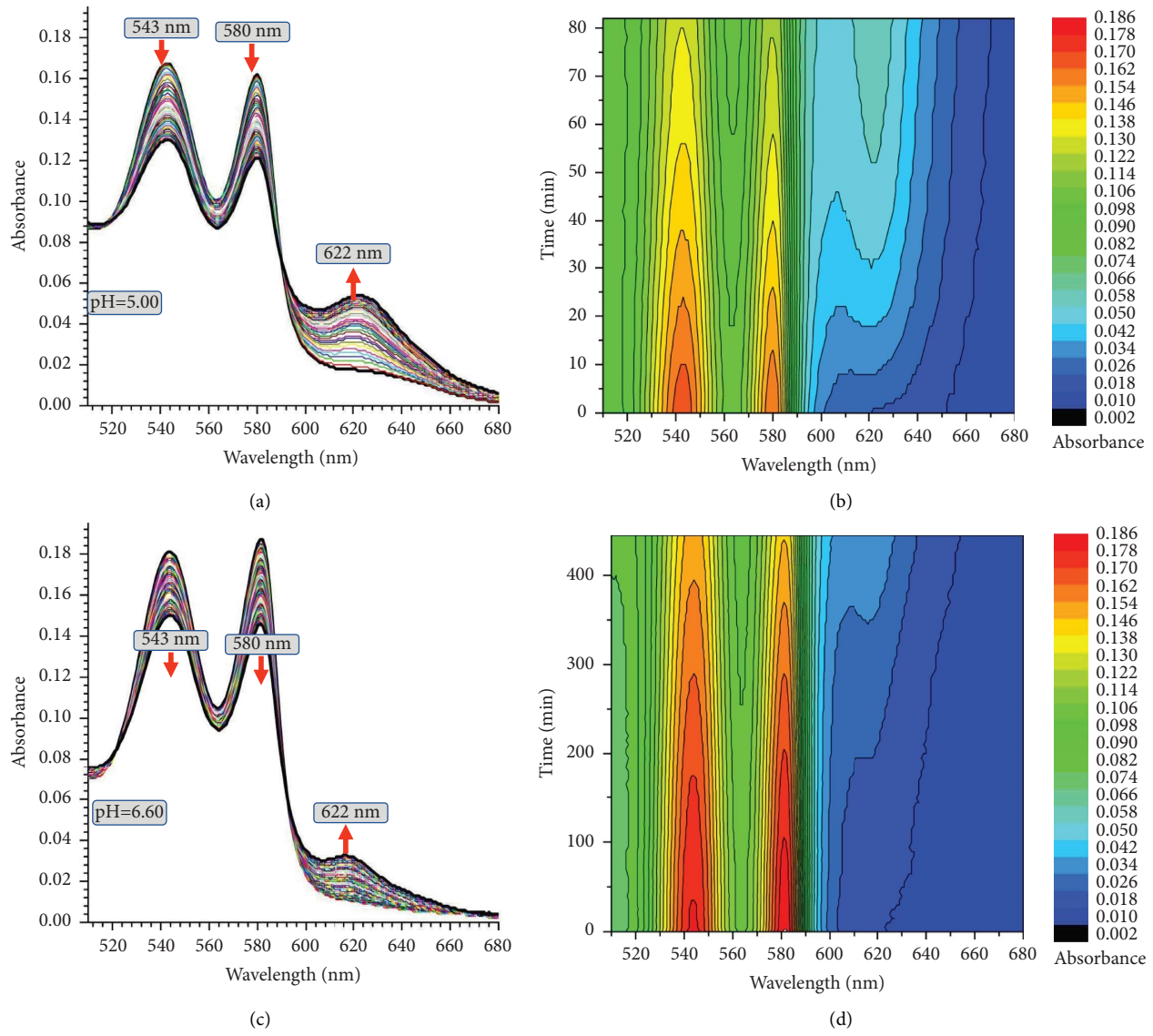

FIGURE 2: UV-Vis spectra of the time evolution for the reaction between oxy-Mb and H_2S (reaction (1b)) at pH 5.0 (a, b) and 6.6 (c, d) for 80 and 450 minutes, respectively.

in Figure 3(a). Advancing along the reaction coordinate in Figure 3 (O_B-O_A bond distance) of the heme Fe(III)O-$O^{\bullet-}$ complex, the distal oxygen atom (O_A) forms hydrogen bond interaction with the nearby S-H moiety of H_2S. As a result, H_2S is homolytically cleaved, donating a hydrogen atom to the distal oxygen (O_A) to produce Cpd-0 [Fe(III)OOH] and a hydrosulfide radical ($HS^{\bullet}$), Figure 3(b). There is a calculated energy barrier of 23.3 kcal/mol for the process. In this intermediate state, all electrons surrounding the ligand are paired, resulting in a null spin density for the O-H bond in Cpd-0, metastable by 11.2 kcal/mol, Figure 3(b). A proton transfer from $His64_{\varepsilon\delta}$ is energetically favorable by 5 kcal/mol, resulting in the formation of a water molecule and the hypervalent Cpd-I radical [Fe(IV)=$O^{+\bullet}$] intermediate, as illustrated in Figure 3(c).

The breaking of the O-O bond of Cpd-0, seen in Figure 4(a), reveals that the spin density is distributed primarily over the β-β double bond of the C_3 and C_2 carbon of the heme pyrrole B. Spin density is also found over the porphyrin central iron atom. This configuration of delocalized electrons over the heme and iron is consistent with the heme ferryl Cpd-I. The short-lived heme Fe(IV)=$O^{+\bullet}$ radical is extinguished by the immediate integration of the $HS^{\bullet}$ radical into the heme group, resulting in the formation of the heme ferryl Cpd-II, Fe(IV)=O, and the episulfide group attached to the β-β double bond of heme pyrrole B, Figure 4(b). The process is accompanied by an energy drop of 32.7 kcal/mol (Figure 3(d)). The formation of the 3-member ring isomer (S_A), seen in Figure 4(c), unravels a series of proton exchanges between the sulfur, a water molecule, and $His64_{\varepsilon\delta}$. The structure is energetically favored over the opened-ring episulfide conformation by 20.8 kcal/mol (Figure 3(e)).

As the three-member ring closes (Figure 4(c)), a proton is transferred from ring-opened episulfide to the bridging water molecule, which simultaneously transfers another

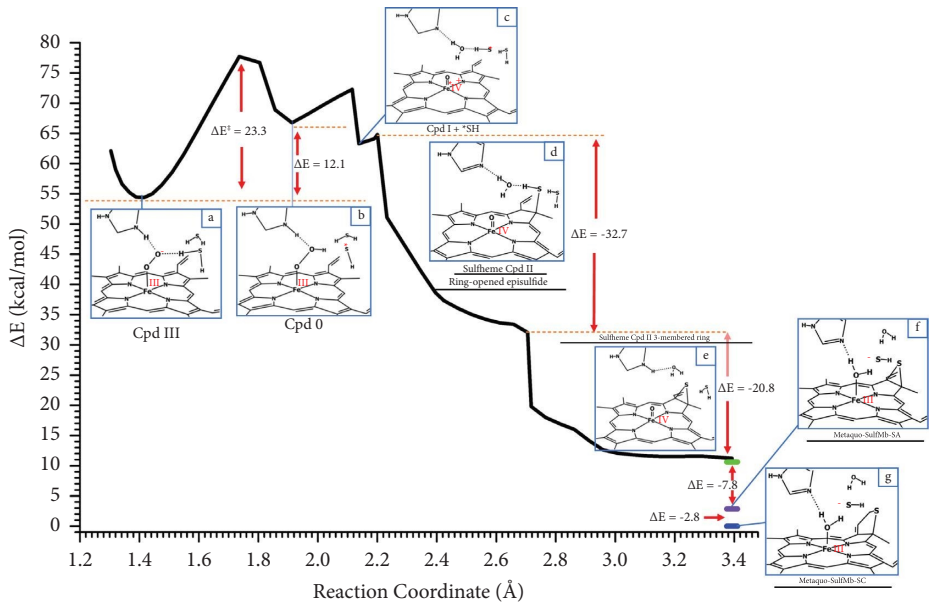

Figure 3: Energetically favorable reaction upon oxy-Mb interaction with H_2S to produce met-aquo-sulfMb.

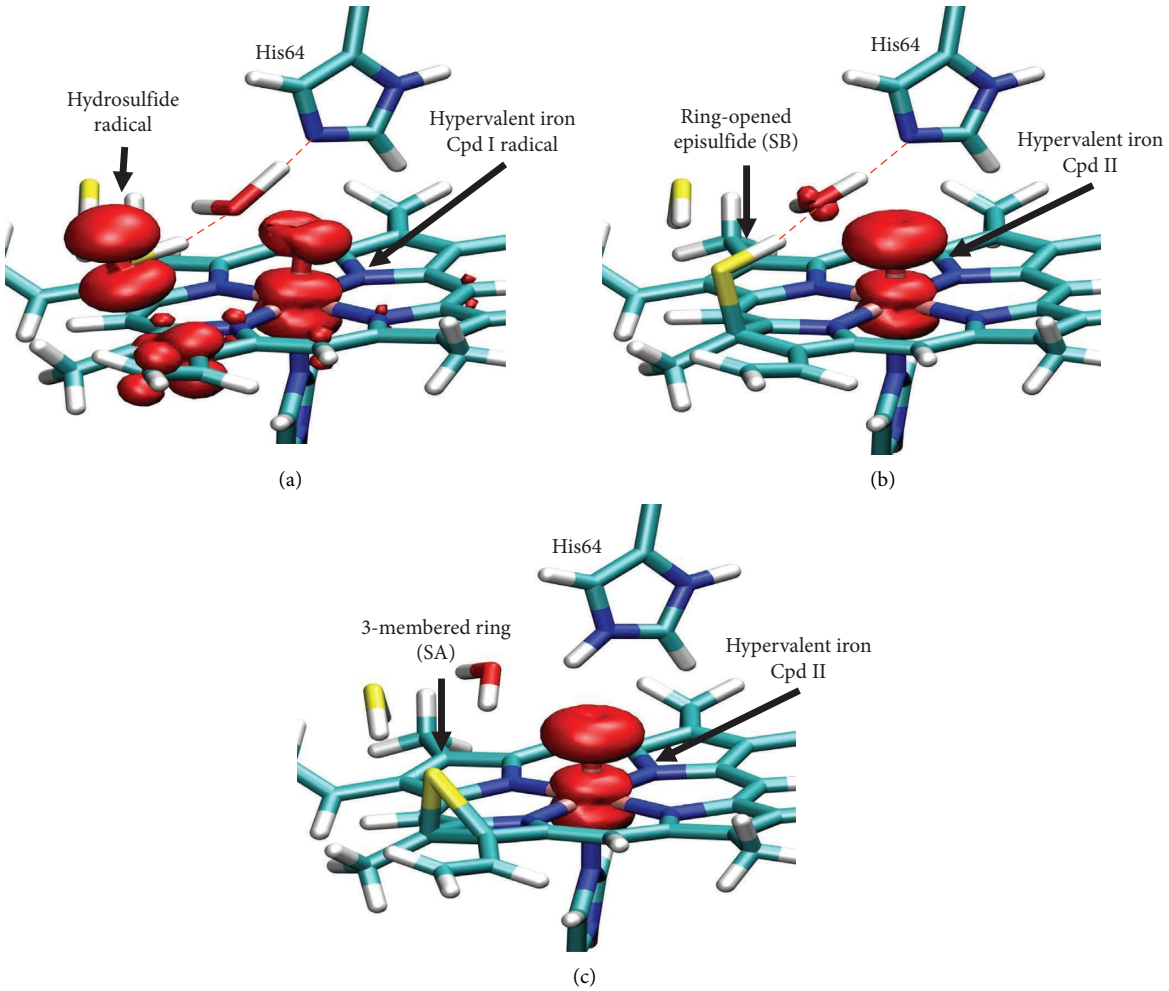

Figure 4: (a) Water and transient Cpd-I formation over the heme group. Spin density is primarily located over the pyrrole B side of the heme. (b) Integrating the $HS^{\bullet}$ radical into the heme led to the mutual annihilation of the radicals and ring-opened episulfide S_B formation. (c) 3-member ring structure; the closing of the ring sets a proton relay between the adjacent water molecule and the distal $His64_{\varepsilon\delta}$.

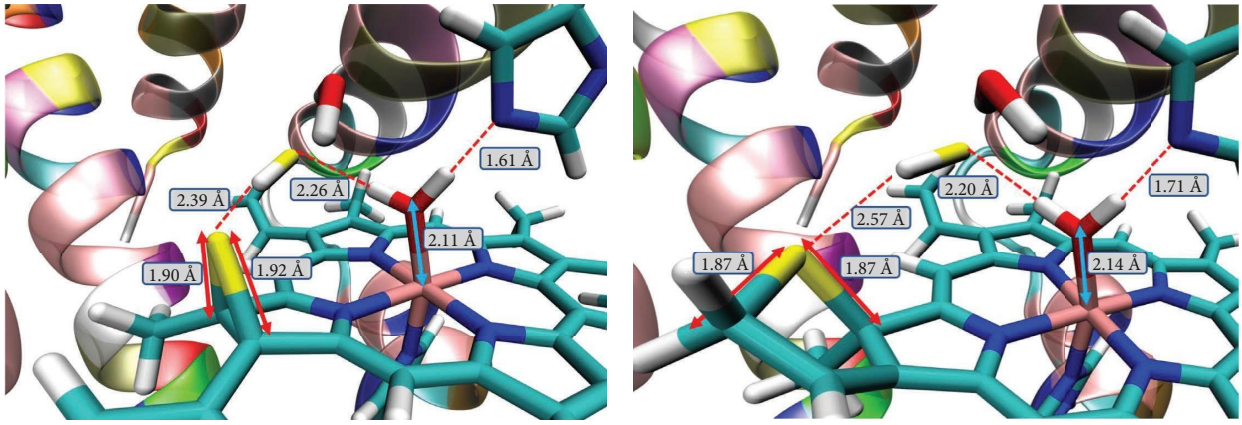

(a) (b)

Figure 5: (a) 3-membered ring and (b) 5-membered ring isomeric structures.

proton to His64$_{\varepsilon\delta}$. This process is energetically favorable by −7.8 kcal/mol, resulting in the formation of the met-aquo-sulfMbS_c species and the SH^- anion (Figure 3(f)). Concurrently, steric effects from the departing water molecule result in the integration of spin density into the heme group via sulfheme isomeric structure formation. The S_C isomeric structure, Figure 3(f), is favored over the S_A arrangement by only −2.8 kcal/mol. As shown in Figure 5, geometrical flexibility and increased conjugation in the heme porphyrin π system, facilitated by the 5-membered ring, may contribute to the structural preference. The preference for this conformation is consistent with our previous work, with a met-aquo Mb analog and hydrogen sulfide (reaction (1a)) [53, 59]. The orientation of the water molecule allows it to function as a bridge between the hydrosulfide and His64$_{\varepsilon\delta}$.

The mutual extinction of the short-lifetime intermediates, Cpd-I and thiyl radical ($HS^\bullet$), leads to a potential energy drop of −69.1 kcal/mol from Cpd-0 to met-aquo-sulfMb. Overall, the formation of the water molecule during the breaking of Cpd-0 O-O bond reveals a concerted proton relay. The pH-dependent triplet state and the His64$_{\varepsilon\delta}$ proton relay are responsible for these specific reaction pathways and the stability of the final products. Also, the mechanism presented in Figure 3 is analogous to the oxy-heme open-shell singlet biradical state. The calculated potential energy profiles do indicate some differences, given that in oxy-Mb His64$_{\varepsilon\delta}$ interaction with H_2S, the triplet state is favored by 31.0 kcal/mol, while hydrogen sulfide stabilizes the complex by 7.0 kcal/mol in the singlet scenario.

3.3. Sulfheme Pathways: Analogous but Exclusive. Interestingly, the sulfheme formation mechanisms, presented in Figure 1S (reaction (1a)) and Figure 3 (reaction (1b)), respectively, show different heme intermediates and energy barriers towards heme Cpd-0. Furthermore, both reactions show a diverse mechanism to produce the thiyl radical, $HS^\bullet$. In the former case, the reaction between Cpd-0 (Heme Fe(III)-OOH) and H_2S produces the radical. In the latter scenario, the reaction between Cpd-III (Fe(III)O-$O^{\bullet-}$ and H_2S leads to the species. Yet in both cases, favorable potential energy pathways of −135.3 kcal/mol and −69.1 kcal/mol come from the thiyl radical species attacking the β-β double bond of heme pyrrole B to produce the sulfheme structure (S_C). Although the mechanism to generate $HS^\bullet$ differs from the model proposed by Nicholls [57], the calculated energetic data supported its presence. Thus, the heme iron oxidation state [FeIII) or Fe(II)], coordinated ligand (H_2O_2 or O_2), singlet or triplet spin states, and pH define the number of electrons available for the reaction processes. Furthermore, the hydrogen bond interactions between heme Fe(III)-H_2O_2 or heme Fe(II)-O_2, heme distal His64, and H_2S also regulate the process.

Table 1 summarizes the intermediates and energy of met-aquo-Mb [Fe(III)] + H_2O_2 and H_2S (reaction (1a)) and oxy-Mb[Fe(II)] in the presence of H_2S (reaction (1b)) to produce sulfheme structure S_C, Figures 1S and 3. In reaction (1a), the energetic barrier for the hydrogen bonding ferric hydroperoxyl moiety to heme compound 0 [Fe(III)-OOH, Cpd-0] is only 1.9 kcal/mol (Figures 1S-A and 1S-B). While in reaction 1b (Figures 3(a) and 3(b)), transition from heme Cpd-III to heme Cpd-0 is accompanied by the synchronized transformation to higher energy (23.3 kcal/mol), transient state [Fe(III)O-$O^{-\bullet}$]. The homolytic cleavage of H_2S follows the generation of a favorable (−11.2 kcal/mol) intermediate, Cpd-0, and a transient thiyl radical ($HS^\bullet$) (Figure 3(b)). Furthermore, reaction (1a) (Figures 1S–1C) shows a favorable (−48.6 kcal/mol) hydrogen transfer route from H_2S to Fe(III)−OOH, heme compound 0 complex, resulting in the homolytic cleavage of the O−O and S−H bonds to form the heme ferryl compound II [Fe(IV)=O], a reactive thiyl radical ($HS^\bullet$), and a water molecule.

Subsequent addition of $HS^\bullet$ to the pyrrole B carbon of heme compound II, [heme Fe(IV)=O], continues to lower the reaction energy (−16.3 kcal/mol) (Figures 1S–1D) to a metastable ring-opened episulfide (S_B). The process allows the formation (−73.3 kcal/mol) of met-aquo-heme Fe(III) three-membered thiochlorinring (S_A) (Figures 1S–1E). The five-membered thiochlorin structure is formed (S_C) with a small barrier of 2.9 kcal/mol (Figures 1S–1E). The mechanism progression generates a favorable (−135.3 kcal/

Table 1: Intermediates and energy of met-aquo-Mb [Fe(III)] + H_2O_2 and H_2S (reaction (1a)) and oxy-Mb[Fe(II)] in the presence of H_2S (reaction (1b)) to produce S_C.

Reaction (1a) intermediates	Energy reaction (1a) intermediates	Reaction (1b) intermediates	Energy reaction (1b) intermediates
Heme Fe(III)-H_2O_2/H_2S	Not present	Fe(III)O-O^-Cpd-III/H_2S	−31.0 kcal/mol
Heme Fe(III)-OOH, Cpd-0	Transition and formation +1.9 (kcal/mol)	Heme Fe(III)-OOH, Cpd-0, and $HS^\bullet$	Transition +23.3 kcal/mol formation −11.2 kcal/mol
Heme Fe(IV)=$O^{+\bullet}$Cpd-I	Not present	Heme Fe(IV)=$O^{+\bullet}$Cpd-I	−5.0 kcal/mol
Heme Fe(IV)=O Cpd-II and $HS^\bullet$	−48.6 kcal/mol	Heme Fe(IV)=O Cpd-II and ring-opened episulfide (S_B)	−32.7 kcal/mol
Heme ring-opened episulfide (S_B)	−16.3 kcal/mol	Present in the previous step	Present in the previous step
Heme Fe(III)H_2O three-membered thiochlorin ring (S_A)	−73.3 kcal/mol	Heme Fe(III)H_2O three-membered thiochlorin ring (S_A) and SH anion (SH^-)	−28.6 kcal/mol (−20.8, −7.8 kcal/mol)
Heme Fe(III)H_2O five-membered thiochlorin (S_C)	+2.9 kcal/mol	Heme Fe(III)H_2O five-membered thiochlorin (S_C)	−2.8 kcal/mol
Heme Cpd-0 to sulfheme (S_C)	−135.3 kcal/mol	Heme Cpd-0 to sulfheme (S_C)	−69.1 kcal/mol

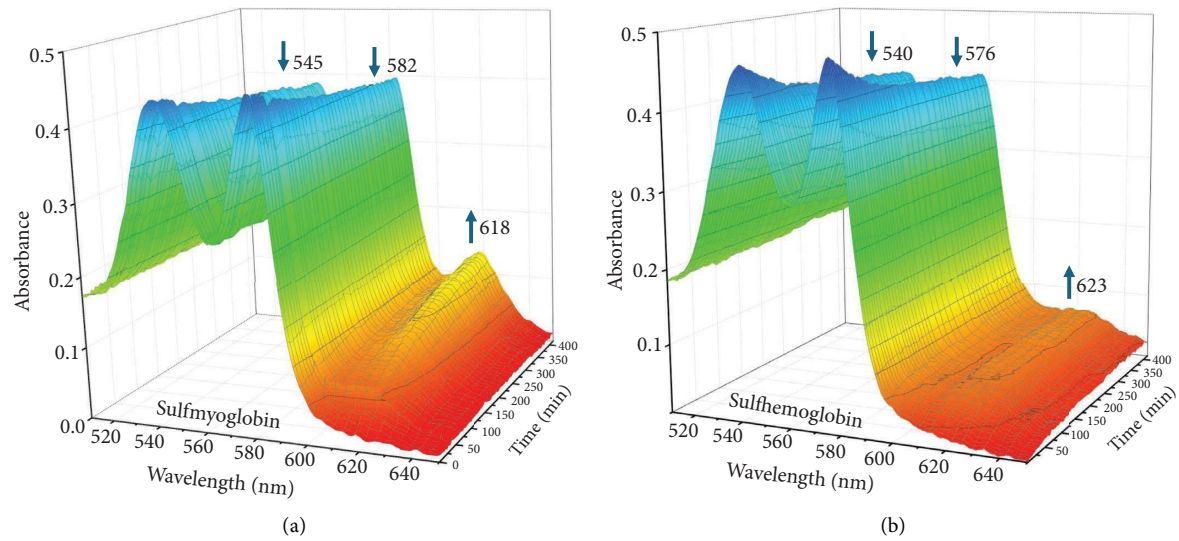

FIGURE 6: Sulfmyoglobin (a) and sulfhemoglobin (b) UV-Vis spectra upon reaction of Mb (55 μM) and Hb (55 μM) with hydrogen sulfide solution (165 μM).

mol) pathway for sulfheme. However, in reaction (1b) (Figure 3(c)), the proton transfer from His64 to the Fe(III)–OOH is associated with a 5 kcal/mol barrier and a transient hypervalent heme Cpd-I radical. This short-lived radical conformation is extinguished by the immediate integration of the thiyl radical into the heme group. The process leads to a potential energy change of −32.7 kcal/mol upon formation of the Cpd-II and the ring-opened episulfide (Figure 3(d)). The presence of the 3-member ring, S_A, is energetically favored over the opened-ring episulfide by −20.8 kcal/mol (Figure 3(e)). A favorable potential energy change of −7.8 kcal/mol is calculated to form met-aquo-sulfMbS_c species and the SH^- anion. The S_C isomeric five-member ring structure is favored over the S_A arrangement by only −2.8 kcal/mol. There is a favorable potential energy decrease, −69.1 kcal/mol, from Cpd-0 to sulfMb (S_C). A primary conclusion from these results is that these reactions primarily differ mechanistically and energetically towards Cpd-0 formation. Yet, the sulfheme product and the intermediate states, except Cpd-I formation, are essentially the same [53, 59, 62].

3.4. SulfMb and SulfHb Formation: Insight of the Charge Transfer Band Intensity. Figure 6 shows sulfMb and sulfHb formation from the reaction between oxy-Mb and oxy-Hb with H_2S under the same experimental conditions of 0.05 mM HEPES buffer solution, pH 7.4, and five hours of reaction time. Both Q electronic transitions at 540 nm and 580 nm regions present similar intensities assigned to π to π^* excitations [42, 45, 50, 57]. At the same time, the 620 nm region is characterized by π to dπ (dyz, dxz) charge transfer transitions [53].

Therefore, the absorption ratios of the 620 nm and 580 nm regions (A_{620}/A_{580}) have been used to estimate the sulfheme reaction yields. In addition, electron paramagnetic resonance (EPR) measurements have been used to determine sulfheme absolute yield [42, 46, 55, 98–100]. Figure 6 indicates that sulfHb presents smaller (A_{623}/A_{576}) ratios than sulfMb (A_{618}/A_{582}). Factors producing this behavior include (i) sulfheme synthesis techniques, (ii) reaction time, (iii) sulfheme ligand species, (iv) autoxidation processes, and (v) pH. However, the 623 nm sulfHb intensity (Figure 6(b)) is also influenced by the tetrameric nature of oxy-Hb [42, 46, 53, 55, 98–100]. Experimentally, 80% yields have been obtained for pure sulfHb formation. Under these circumstances, the process is initiated from the reaction between met-aquo-Hb and H_2O_2, followed by the complete sulfheme product oxidation using potassium ferricyanide, $K_3Fe(CN)_6$, to obtain the hydroxyl sulfheme [hemeFe(III)-OH] form at pH 8.5. The species undergoes reduction to deoxy-sulfheme, and when exposed to high molecular oxygen pressure, oxy-sulfHb is produced [42, 46, 53, 55, 98–101]. However, as time evolves, the autoxidation process leads to hydroxyl-, deoxy-, and oxy-sulfheme resulting in the intensity decrease and a broad 623 nm band. Moreover, not all monomeric subunits of Hb generate sulfheme, suggesting a mixture of heme and sulfheme within the Hb tetrameric structure. The generation of different sulfHb centers, from one to four, also limits, relative to sulfHb, the intensity of the 623 nm region. These results have been beneficial in explaining the 10% to 15% sulfHb yield from a patient-derived sample [98–100]. Therefore, the lower 623 nm intensity of sulfHb suggests that the approach can be further used, with caution, to comprehend and directly detect the landscape of these sulfheme derivatives in human tissues and red blood cells. Otherwise, the result could be interpreted as lacking sulfHb formation, contrary to the literature observations [13, 32–41].

4. Conclusions

Experimentally, the reaction between oxy-Mb and H_2S at pH 5.00 and 6.60 showed that the distal doubly protonated tautomer His64$_{\varepsilon\delta}$ in the heme active site promotes faster sulfMb formation than the mono-protonated analog, His64$_{\varepsilon}$.

At more acidic pH, the 622 nm charge transfer band, characteristic of sulfMb, increases in intensity, reaching its maximum absorbance in 30 minutes, while the process at the higher pH takes 350 minutes. Thus, as pH increases, the transformation from the triplet state to the singlet state is preferred, explaining the intensity decrease of the 622 nm transition. Also, results show that in sulfMb and sulfHb, the differences between the 618 nm and 623 nm transition intensities could be attributed to partial sulfheme presence in the heme groups of the oxy-Hb tetrameric protein. Further research is required to understand the sulfheme derivative formation in red blood cells. Moreover, employing hybrid QM/MM methods aids in elucidating the mechanism and energetics governing the reaction between oxy-Mb and H_2S (reaction (1b)) in aqueous media, leading to the formation of sulfMb. The data indicated that pH changes and the protonation state of the distal His 64 regulate the Cpd-III triplet population that drives the intermediates (Table 1) to favorable energetics (−69.1 kcal/mol) towards sulfMb (S_C) formation. The hydrogen bonding network between $His64_{\varepsilon\delta}$, heme $Fe(II)O_2$, and H_2S is responsible for the phenomenon. Furthermore, Table 1 presents the energetics of reaction intermediates for the interaction between met-aquo-Mb [Fe(III)] and H_2O_2 in the presence of H_2S, resulting in sulfMb formation (reaction (1a)). Notably, the process exhibits a favorable sulfheme formation (S_C) with an energy of −135.3 kcal/mol. Furthermore, Table 1 summarizes intermediate pathways for oxy-Mb and H_2S (reaction (1b)) and met-aquo Mb, hydrogen peroxide, and H_2S (reaction (1a)) processes. The results support the hypothesis that the energy barrier towards the heme Cpd-0 formation is responsible for the energetic difference between these two unique reactions to produce sulfMb. Likewise, both mechanisms suggest, albeit with different energetics, that the formation of the thiyl radical $HS^{\bullet}$ is the key species driving the attack on the β-β double bond of heme pyrrole B, leading to a five-member ring sulfheme structure. However, the experimental determination of whether the final stable products in sulfMb and sulfHb are exclusively met-aquo-sulfMb and aquo-sulfHb or a mixture of various sulfheme-ligated species, including hydrogen sulfide as a ligand bound to the heme group, remains a subject of controversy [56, 63, 102, 103].

Data Availability

The data used to support the findings of this study are included within the article. Additional information is available upon request to Ángel D. Rodriguez-Mackenzie and Lysmarie Santos Velazquez.

Conflicts of Interest

The authors declare that they have no conflicts of interest.

Acknowledgments

This research was supported by PR-INBRE, funded by NIH/NIGMS, under grant no. P20GM103475. In addition, we thank the support of the Alfred P. Sloan Foundation Graduate Scholarship Program.

Supplementary Materials

Figure 1S: The energy barrier from ferric hydroperoxyl moiety (Figure 1S-A) to heme compound 0 (Figure 1S-B) is only 1.9 kcal/mol. There is an energetically favorable hydrogen transfer, −48.6 kcal/mol, from H_2S to Fe(III)−OOH (Figures 1S-1C). The heme compound 0 complex enables the homolytic cleavage of the O−O and S−H bonds to form heme ferryl compound-II, a reactive thiyl radical ($HS^{\bullet}$), and a water molecule [104]. Figures 1S–1D show the subsequent addition of $HS^{\bullet}$ to the pyrrole B carbon of heme compound-II, which continues to lower the reaction energy (−16.3 kcal/mol) resulting in a metastable ring-opened episulfide (SB). The reaction is followed by the formation (−73.3 kcal/mol) of met-aquo-heme Fe(III) three-membered thiochlorin ring (SA), Figures 1S–1E. Finally, the five-membered thiochlorin structure is formed (SC) with a small 2.9 kcal/mol barrier, Figure 1S–1F. Figure 2S: Sperm Whale Mb solvated in a 71 $Å^3$ water cube. Including the entire heme group, O_2 ligand, two H_2S molecules, distal amino acid residues; His64, Val68, Phe43, Arg29, and proximal His93. (*Supplementary Materials*)

References

[1] S. Rajendran, X. Shen, J. Glawe, G. K. Kolluru, C. G. Kevil, and G. K. Kolluru, "Nitric oxide and hydrogen sulfide regulation of ischemic vascular growth and remodeling," *Comprehensive Physiology*, vol. 9, no. 3, pp. 1213–1247, 2019.

[2] K. R. Olson, "Is hydrogen sulfide a circulating gasotransmitter in vertebrate blood?" *Biochimica et Biophysica Acta (BBA) Bioenergetics*, vol. 1787, no. 7, pp. 856–863, 2009.

[3] R. Wang, "Physiological implications of hydrogen sulfide: a whiff exploration that blossomed," *Physiological Reviews*, vol. 92, no. 2, pp. 791–896, 2012.

[4] M. R. Hellmich, C. Coletta, C. Chao, and C. Szabo, "The therapeutic potential of cystathionine β-synthetase/hydrogen sulfide inhibition in cancer," *Antioxidants and Redox Signaling*, vol. 22, no. 5, pp. 424–448, 2015.

[5] J. C. Mathai, A. Missner, P. Kugler et al., "No facilitator required for membrane transport of hydrogen sulfide," *Proceedings of the National Academy of Sciences*, vol. 106, no. 39, pp. 16633–16638, 2009.

[6] S. Zhang, C. Pan, F. Zhou et al., "Hydrogen sulfide as a potential therapeutic target in fibrosis," *Oxidative Medicine and Cellular Longevity*, vol. 2015, Article ID 593407, 12 pages, 2015.

[7] G. Renieris, K. Katrini, C. Damoulari et al., "Serum hydrogen sulfide and outcome association in pneumonia by the SARS-CoV-2 Coronavirus," *Shock*, vol. 54, no. 5, pp. 633–637, 2020.

[8] G. Yang, "H_2S as a potential defense against COVID-19?" *American Journal of Physiology Cell Physiology*, vol. 319, no. 2, pp. C244–C249, 2020.

[9] F. Gorini, S. Del Turco, L. Sabatino, M. Gaggini, and C. Vassalle, "H_2S as a bridge linking inflammation, oxidative stress, and endothelial biology: a possible defense in the fight against SARS-CoV-2 infection?" *Biomedicines*, vol. 9, no. 9, p. 1107, 2021.

[10] M. Iciek, A. Bilska-Wilkosz, M. Kozdrowicki, and M. Górny, "Reactive sulfur compounds in the fight against COVID-19," *Antioxidants*, vol. 11, no. 6, p. 1053, 2022.

[11] J. L. Wallace and R. Wang, "Hydrogen sulfide-based therapeutics: exploiting a unique but ubiquitous gasotransmitter," *Nature Reviews Drug Discovery*, vol. 14, no. 5, pp. 329–345, 2015.

[12] E. Zaorska, L. Tomasova, D. Koszelewski, R. Ostaszewski, and M. Ufnal, "Hydrogen sulfide in pharmacotherapy, beyond the hydrogen sulfide-donors," *Biomolecules*, vol. 10, no. 2, p. 323, 2020.

[13] M. Whiteman, S. Le Trionnaire, M. Chopra, B. Fox, and J. Whatmore, "Emerging role of hydrogen sulfide in health and disease: critical appraisal of biomarkers and pharmacological tools," *Clinical Science*, vol. 121, no. 11, pp. 459–488, 2011.

[14] T. Lu, G. Cui, S. Y. Peng, X. Wu, and G. Chen, "Research progress of hydrogen sulfide in Alzheimer's disease from laboratory to hospital: a narrative review," *Medical Gas Research*, vol. 10, no. 3, pp. 125–129, 2020.

[15] B. V. Nagpure and J.-S. Bian, "Brain, learning, and memory: role of H_2S in neurodegenerative diseases," *Handbook of Experimental Pharmacology*, vol. 230, pp. 193–215, 2015.

[16] N. Yang, Y. Liu, T. Li, and Q. Tuo, "Role of hydrogen sulfide in chronic diseases," *DNA and Cell Biology*, vol. 39, no. 2, pp. 187–196, 2020.

[17] T. Merz, O. McCook, C. Brucker et al., "H_2S in critical illness-A new horizon for sodium thiosulfate?" *Biomolecules*, vol. 12, no. 4, p. pp543, 2022.

[18] H. J. Sun, Z. Y. Wu, X. W. Nie, and J. S. Bian, "Role of endothelial dysfunction in cardiovascular diseases: the link between inflammation and hydrogen sulfide," *Frontiers in Pharmacology*, vol. 10, p. 1568, 2019.

[19] M. Xu, X. Liu, P. Bao, Y. J. Wang, J. Lu, and Y. J. Liu, "H_2S protects against immobilization-induced muscle atrophy via reducing oxidative stress and inflammation," *Frontiers in Physiology*, vol. 13, Article ID 844539, 2022.

[20] L. Li, Z. He, Y. Zhu, Q. Shen, S. Yang, and S. Cao, "Hydrogen sulfide suppresses skin fibroblast proliferation *via* oxidative stress alleviation and necroptosis inhibition," *Oxidative Medicine and Cellular Longevity*, vol. 2022, Article ID 7434733, 16 pages, 2022.

[21] R. Parsanathan and S. K. Jain, "Hydrogen sulfide regulates irisin and glucose metabolism in myotubes and muscle of HFD-fed diabetic mice," *Antioxidants*, vol. 11, no. 7, p. 1369, 2022.

[22] Y. Sun, C. Tang, H. Jin, and J. Du, "Implications of hydrogen sulfide in development of pulmonary hypertension," *Biomolecules*, vol. 12, no. 6, p. 772, 2022.

[23] A. Ahmad, "Physiological, pathological and pharmacological interactions of hydrogen sulphide and nitric oxide in the myocardium of rats with left ventricular hypertrophy," *Current Issues in Molecular Biology*, vol. 44, no. 1, pp. 433–448, 2022.

[24] S. Zhu, X. Li, B. Dang et al., "Hydrogen sulfide protects retina from blue light-induced photodamage and degeneration via inhibiting ROS-mediated ER stress-CHOP apoptosis signal," *Redox Report*, vol. 27, pp. 100–110, 2022.

[25] K. Barrow, Y. Wang, R. Yu, J. Zhu, and G. Yang, "H_2S protects from oxidative stress-driven ACE2 expression and cardiac aging," *Molecular and Cellular Biochemistry*, vol. 477, no. 5, pp. 1393–1403, 2022.

[26] D. D. Wu, E. E. Ngowi, Y. K. Zhai et al., "Role of hydrogen sulfide in oral disease," *Oxidative Medicine and Cellular Longevity*, vol. 2022, Article ID 1886277, 14 pages, 2022.

[27] Y. Feng, V. Prokosch, and H. Liu, "Current perspective of hydrogen sulfide as a novel gaseous modulator of oxidative stress in glaucoma," *Antioxidants*, vol. 10, no. 5, p. 671, 2021.

[28] D. Lu, L. Wang, G. Liu et al., "Role of hydrogen sulfide in subarachnoid hemorrhage," *CNS Neuroscience and Therapeutics*, vol. 28, no. 6, pp. 805–817, 2022.

[29] F. Akbarian, M. Tavalaee, M. Dattilio, and M. H. Nasr-Esfahani, "Down-regulated expression of cystathionine β-synthase and cystathionine γ-lyase in varicocele, and infertile men: a case-control study," *Cell J*, vol. 24, no. 4, pp. 176–181, 2022.

[30] Y. Huang, G. Wang, Z. Zhou et al., "Endogenous hydrogen sulfide is an important factor in maintaining arterial oxygen saturation," *Frontiers in Pharmacology*, vol. 12, Article ID 677110, 2021.

[31] Q. Xiao, L. Xiong, J. Tang, L. Li, and L. Li, "Hydrogen sulfide in skin diseases: a novel mediator and therapeutic target," *Oxidative Medicine and Cellular Longevity*, vol. 2021, Article ID 6652086, 11 pages, 2021.

[32] A. Rangan, M. E. Savedra, C. Dergam-Larson et al., "Interpreting Sulfhemoglobin and methemoglobin in patients with cyanosis: an overview of patients with M-hemoglobin variants," *The International Journal of Literary Humanities*, vol. 43, no. 4, pp. 837–844, 2021.

[33] A. Tangerman, G. Bongaerts, R. Agbeko, B. Semmekrot, and R. Severijnen, "The origin of hydrogen sulfide in a newborn with sulfhaemoglobin induced cyanosis," *Journal of Clinical Pathology*, vol. 55, no. 8, pp. 631–633, 2002.

[34] A. M. Attia, W. M. Aboulthana, G. M. Hassan, and E. Aboelezz, "Assessment of absorbed dose of gamma rays using the simultaneous determination of inactive hemoglobin derivatives as a biological dosimeter," *Radiation and Environmental Biophysics*, vol. 59, no. 1, pp. 131–144, 2020.

[35] A. M. Attia, F. A. Ibrahim, N. A. Abd El-Latif, S. W. Aziz, S. A. Abdelmottaleb Moussa, and M. S. Elalfy, "Determination of human hemoglobin derivatives," *Hemoglobin*, vol. 39, no. 5, pp. 371–374, 2015.

[36] D. Padovani, A. Hessani, F. Castillo et al., "Sulfheme formation during homocysteine S-oxygenation by catalase in cancers and neurodegenerative diseases," *Nature Communications*, vol. 7, no. 1, Article ID 13386, 2016.

[37] J. L. Burgess, A. P. Hamner, and W. O. Robertson, "Sulfhemoglobinemia after dermal application of DMSO," *Veterinary and Human Toxicology*, vol. 40, no. 2, pp. 87–89, 1998.

[38] A. Zwart, A. Buursma, E. J. van Kampen, and W. G. Zijlstra, "Multicomponent analysis of hemoglobin derivatives with reversed-optics spectrophotometer," *Clinical Chemistry*, vol. 30, no. 3, pp. 373–379, 1984.

[39] E. J. van Kampen and W. G. Zijlstra, "Spectrophotometry of hemoglobin and hemoglobin derivatives," *Advances in Clinical Chemistry*, vol. 23, pp. 199–257, 1983.

[40] N. Fogh-Andersen, O. Siggaard-Andersen, F. C. Lundsgaard, and P. D. Wimberley, "Diode-array spectrophotometry for simultaneous measurement of hemoglobin pigments," *Clinica Chimica Acta*, vol. 166, no. 2-3, pp. 283–289, 1987.

[41] P. Demedts, A. Wauters, M. Watelle, and H. Neels, "Pitfalls in discriminating sulfhemoglobin from methemoglobin," *Clinical Chemistry*, vol. 43, no. 6, pp. 1098-1099, 1997.

[42] J. A. Berzofsky, J. Peisach, and W. Blumberg, "SulfHeme proteins: II. The reversible oxygenation of ferrous sulfmyoglobin," *Journal of Biological Chemistry*, vol. 246, no. 23, pp. 7366–7372, 1971.

[43] M. Noor and E. Beutler, "Acquired sulfhemoglobinemia. An underreported diagnosis?" *Western Journal of Medicine*, vol. 169, no. 6, pp. 386–389, 1998.

[44] C. Wu and M. A. Kenny, "A case of sulfhemoglobinemia and emergency measurement of Sulfhemoglobin with an OSM3 CO-oximeter," *Clinical Chemistry*, vol. 43, no. 1, pp. 162–166, 1997.

[45] E. A. Johnson, "The reversion to haemoglobin of sulph-haemoglobin and its coordination derivatives," *Biochimica et Biophysica Acta (BBA) Protein Structure*, vol. 207, no. 1, pp. 30–40, 1970.

[46] J. A. Berzofsky, J. Peisach, and W. E. Blumberg, "Sulfheme proteins," *Journal of Biological Chemistry*, vol. 246, no. 10, pp. 3367–3377, 1971.

[47] J. A. Berzofsky, J. Peisach, and B. L. Horecker, "Sulfheme proteins," *Journal of Biological Chemistry*, vol. 247, no. 12, pp. 3783–3791, 1972.

[48] S. V. Evans, B. P. Sishta, A. G. Mauk, and G. D. Brayer, "Three-dimensional structure of cyanomet-sulfmyoglobin C," *Proceedings of the National Academy of Sciences*, vol. 91, no. 11, pp. 4723–4726, 1994.

[49] M. J. Chatfield, G. N. La Mar, and R. J. Kauten, "Proton NMR characterization of isomeric sulfmyoglobins: preparation, interconversion, reactivity patterns, and structural features," *Biochemistry*, vol. 26, no. 22, pp. 6939–6950, 1987.

[50] J. A. Berzofsky, J. Peisach, and J. Alben, "Sulfheme Proteins III. Carboxysulfmyoglobin: the relation between electron withdrawal from iron and ligand binding," *Journal of Biological Chemistry*, vol. 247, no. 12, pp. 3774–3782, 1972.

[51] R. Timkovich and M. R. Vavra, "Proton NMR spectroscopy of sulfmyoglobin," *Biochemistry*, vol. 24, no. 19, pp. 5189–5196, 1985.

[52] L. L. Bondoc, M. H. Chau, M. A. Price, and R. Timkovich, "Structure of a stable form of sulfheme," *Biochemistry*, vol. 25, no. 26, pp. 8458–8466, 1986.

[53] H. Arbelo-López, A. D. Rodriguez-Mackenzie, E. M. Roman-Morales, T. Wymore, and J. López-Garriga, "Charge transfer and π to $\pi*$ transitions in the visible spectra of sulfheme met isomeric structures," *Journal of Physical Chemistry B*, vol. 122, no. 19, pp. 4947–4955, 2018.

[54] H. O. Michel, "A study of Sulfhemoglobin," *Journal of Biological Chemistry*, vol. 126, no. 1, pp. 323–348, 1938.

[55] S. H. Libardi, H. Pindstrup, D. R. Cardoso, and L. H. Skibsted, "Reduction of ferryl myoglobin by hydrogen sulfide. Kinetics in relation to meat greening," *Journal of Agricultural and Food Chemistry*, vol. 61, no. 11, pp. 2883–2888, 2013.

[56] E. Román-Morales, R. Pietri, B. Ramos-Santana, S. N. Vinogradov, A. Lewis-Ballester, and J. López-Garriga, "Structural determinants for the formation of sulfheme-protein complexes," *Biochemical and Biophysical Research Communications*, vol. 400, no. 4, pp. 489–492, 2010.

[57] P. Nicholls, "The Formation and properties of sulphmyoglobin and sulphcatalase," *Biochemical Journal*, vol. 81, no. 2, pp. 374–383, 1961.

[58] S. Nakamura, M. Nakamura, I. Yamazaki, and M. Morrison, "Reactions of ferryl lactoperoxidase (compound II) with sulfide and sulfhydryl compounds," *Journal of Biological Chemistry*, vol. 259, no. 11, pp. 7080–7085, 1984.

[59] H. D. Arbelo-Lopez, N. A. Simakov, J. C. Smith, J. Lopez-Garriga, and T. Wymore, "Homolytic cleavage of both heme-bound hydrogen peroxide and hydrogen sulfide leads to the formation of sulfheme," *Journal of Physical Chemistry B*, vol. 120, no. 30, pp. 7319–7331, 2016.

[60] K. Ratanasopa, M. B. Strader, A. I. Alayash, and L. Bulow, "Dissection of the radical reactions linked to fetal hemoglobin reveals enhanced pseudoperoxidase activity," *Frontiers in Physiology*, vol. 6, p. 39, 2015.

[61] W. De Jesús-Bonilla, A. Cruz, A. Lewis et al., "Hydrogen-bonding conformations of tyrosine B10 tailor the heme-protein reactivity of ferryl species," *Journal of Biological Inorganic Chemistry*, vol. 11, no. 3, pp. 334–342, 2006.

[62] A. D. Rodriguez-Mackenzie, H. D. Arbelo-Lopez, T. Wymore, and J. Lopez-Garriga, "A reaction pathway to compound 0 intermediates in oxy-myoglobin through interactions with hydrogen sulfide and His64," *Journal of Molecular Graphics and Modelling*, vol. 94, Article ID 107465, 2020.

[63] R. Pietri, A. Lewis, R. G. León et al., "Factors controlling the reactivity of hydrogen sulfide with hemeproteins," *Biochemistry*, vol. 48, no. 22, pp. 4881–4894, 2009.

[64] M. E. Antonini and M. Brunori, *The Derivatives of Ferric Hemoglobin and Myoglobin*, North-Holland Publishing Company, Amsterdam, Netherlands, 1971.

[65] H. Chen, M. Ikeda-Saito, and S. Shaik, "Nature of the Fe–O_2 bonding in oxy-myoglobin: effect of the protein," *Journal of the American Chemical Society*, vol. 130, no. 44, pp. 14778–14790, 2008.

[66] H.-P. Hersleth, Y.-W. Hsiao, U. Ryde, C. H. Görbitz, and K. K. Andersson, "The crystal structure of peroxymyoglobin generated through cryoradiolytic reduction of myoglobin compound III during data collection," *Biochemical Journal*, vol. 412, no. 2, pp. 257–264, 2008.

[67] B. R. Brooks, C. L. Brooks, A. D. Mackerell et al., "CHARMM: the biomolecular simulation program," *Journal of Computational Chemistry*, vol. 30, no. 10, pp. 1545–1614, 2009.

[68] A. D. Mackerell, M. Feig, and C. L. Brooks, "Extending the treatment of backbone energetics in protein force fields: limitations of gas-phase quantum mechanics in reproducing protein conformational distributions in molecular dynamics simulations," *Journal of Computational Chemistry*, vol. 25, no. 11, pp. 1400–1415, 2004.

[69] W. L. Jorgensen, J. Chandrasekhar, J. D. Madura, R. W. Impey, and M. L. Klein, "Comparison of simple potential functions for simulating liquid water," *The Journal of Chemical Physics*, vol. 79, no. 2, pp. 926–935, 1983.

[70] F. Autenrieth, E. Tajkhorshid, J. Baudry, and Z. Luthey-Schulten, "Classical force field parameters for the heme prosthetic group of cytochrome C," *Journal of Computational Chemistry*, vol. 25, no. 13, pp. 1613–1622, 2004.

[71] J. P. Ryckaert, G. Ciccotti, and H. J. Berendsen, "Numerical integration of the cartesian equations of motion of a system with constraints: molecular dynamics of n-alkanes," *Journal of Computational Physics*, vol. 23, no. 3, pp. 327–341, 1977.

[72] M. J. Field, "The PDynamo program for molecular simulations using hybrid quantum chemical and molecular mechanical potentials," *Journal of Chemical Theory and Computation*, vol. 4, no. 7, pp. 1151–1161, 2008.

[73] J. J. P. Stewart, "Optimization of parameters for semi-empirical methods V: modification of NDDO approximations and application to 70 elements," *Journal of Molecular Modeling*, vol. 13, no. 12, pp. 1173–1213, 2007.

[74] W. Humphrey, A. Dalke, and K. Schulten, "VMD: visual molecular dynamics," *Journal of Molecular Graphics*, vol. 14, no. 1, pp. 33–38, 1996.

[75] F. Neese, "The ORCA program system," *WIREs Computational Molecular Science*, vol. 2, no. 1, pp. 73–78, 2012.

[76] J. P. Perdew and A. Zunger, "Self-interaction correction to density-functional approximations for many-electron systems," *Physical Review B: Condensed Matter*, vol. 23, no. 10, pp. 5048–5079, 1981.

[77] A. D. Becke, "Density-functional exchange-energy approximation with correct asymptotic behavior," *Physical Review A*, vol. 38, no. 6, pp. 3098–3100, 1988.

[78] J. P. Perdew, "Density-functional approximation for the correlation energy of the inhomogeneous electron gas," *Physical Review B: Condensed Matter*, vol. 33, no. 12, pp. 8822–8824, 1986.

[79] S. Grimme, S. Ehrlich, and L. Goerigk, "Effect of the damping function in dispersion corrected density functional theory," *Journal of Computational Chemistry*, vol. 32, no. 7, pp. 1456–1465, 2011.

[80] S. Grimme, J. Antony, S. Ehrlich, and H. A. Krieg, "A consistent and accurate *ab initio* parametrization of density functional dispersion correction (DFT-D) for the 94 elements H-Pu," *The Journal of Chemical Physics*, vol. 132, no. 15, Article ID 154104, 2010.

[81] A. Schäfer, H. Horn, and R. Ahlrichs, "Fully optimized contracted Gaussian basis sets for atoms Li to Kr," *The Journal of Chemical Physics*, vol. 97, no. 4, pp. 2571–2577, 1992.

[82] A. Schäfer, C. Huber, and R. Ahlrichs, "Fully optimized contracted Gaussian basis sets of triple zeta valence quality for atoms Li to Kr," *The Journal of Chemical Physics*, vol. 100, no. 8, pp. 5829–5835, 1994.

[83] F. Weigend, "Accurate coulomb-fitting basis sets for H to Rn," *Physical Chemistry Chemical Physics*, vol. 8, no. 9, pp. 1057–1065, 2006.

[84] M. Dolg, U. Wedig, H. Stoll, and H. Preuss, "Energy-adjusted ab initio pseudopotentials for the first row transition elements," *The Journal of Chemical Physics*, vol. 86, no. 2, pp. 866–872, 1987.

[85] J. M. L. Martin and A. Sundermann, "Correlation consistent valence basis sets for use with the stuttgart–dresden–bonn relativistic effective core potentials: the atoms Ga–Kr and in–Xe," *The Journal of Chemical Physics*, vol. 114, no. 8, pp. 3408–3420, 2001.

[86] E. F. Valeev, "Libint: A Library for the Evaluation of Molecular Integrals of Many-Body Operators over Gaussian Functions," 2024, http://libint.valeyev.net/.

[87] A. D. Becke, "Density-functional thermochemistry III the role of exact exchange," *The Journal of Chemical Physics*, vol. 98, no. 7, pp. 5648–5652, 1993.

[88] C. Lee, W. Yang, and R. G. Parr, "Development of the colle-salvetti correlation-energy formula into a functional of the electron density," *Physical Review B: Condensed Matter*, vol. 37, no. 2, pp. 785–789, 1988.

[89] G. Brewer, J. Olida, A. M. Schmiedekamp, C. Viragh, and P. Y. Zavalij, "A DFT computational study of spin crossover in iron (III) and iron (II) tripodal imidazole complexes. A comparison of experiment with calculations," *Dalton Transactions*, vol. 47, pp. 5617–5629, 2006.

[90] C. J. Cramer and D. G. Truhlar, "Density functional theory for transition metals and transition metal chemistry," *Physical Chemistry Chemical Physics*, vol. 11, no. 46, pp. 10757–10816, 2009.

[91] S. Yamamoto and H. Kashiwagi, "CASSCF calculation on dioxygen heme complex with extended basis set," *Chemical Physics Letters*, vol. 205, no. 2-3, pp. 306–312, 1993.

[92] A. L. Hansen and L. E. Kay, "Measurement of histidine pKa values and tautomer populations in invisible protein states," *Proceedings of the National Academy of Sciences of the United States of America*, vol. 111, no. 17, pp. 1705–1712, 2014.

[93] R. Zadorozhnyi, S. Sarkar, C. M. QuinN et al., "Determination of histidine protonation states in proteins by fast magic angle spinning NMR," *Frontiers in Molecular Biosciences*, vol. 8, Article ID 767040, 2021.

[94] V. Vaz da Cruz, R. Büchner, M. Fondell, A. Pietzsch, S. Eckert, and A. Föhlisch, "Targeting individual tautomers in equilibrium by resonant inelastic X-ray scattering," *Journal of Physical Chemistry Letters*, vol. 13, no. 10, pp. 2459–2466, 2022.

[95] B. Rabenstein and E. W. Knapp, "Calculated pH-dependent population and protonation of carbon-monoxy-myoglobin conformers," *Biophysical Journal*, vol. 80, no. 3, pp. 1141–1150, 2001.

[96] I. Birukou, R. L. Schweers, and J. S. Olson, "Distal histidine stabilizes bound O_2 and acts as a gate for ligand entry in both subunits of adult human hemoglobin," *Journal of Biological Chemistry*, vol. 285, no. 12, pp. 8840–8854, 2010.

[97] R. M. Esquerra, R. A. Jensen, S. Bhaskaran et al., "The pH dependence of heme pocket hydration and ligand rebinding kinetics in photodissociated carbon-monoxymyoglobin," *Journal of Biological Chemistry*, vol. 283, no. 20, pp. 14165–14175, 2008.

[98] R. J. Carrico, J. Peisach, and J. O. Alben, "The preparation and some physical properties of sulfhemoglobin," *Journal of Biological Chemistry*, vol. 253, no. 7, pp. 2386–2391, 1978.

[99] C. M. Park and R. L. Nagel, "Sulfhemoglobinemia. Clinical and molecular aspects," *New England Journal of Medicine*, vol. 310, no. 24, pp. 1579–1584, 1984.

[100] C. M. Park, R. L. Nagel, W. E. Blumberg, J. Peisach, and R. S. Magliozzo, "Sulfhemoglobin. Properties of partially sulfurated tetramers," *Journal of Biological Chemistry*, vol. 261, no. 19, pp. 8805–8810, 1986.

[101] A. Álvarez-Armenta, R. Pacheco-Aguilar, A. A. López-Zavala et al., "The greening reaction of skipjack tuna (Katsuwonus pelamis) metmyoglobin promoted by free cysteine during thermal treatment," *PeerJ*, vol. 10, Article ID 13923, 2022.

[102] A. Domán, E. Dóka, D. Garai et al., "Interactions of reactive sulfur species with metalloproteins," *Redox Biology*, vol. 60, Article ID 102617, 2023.

[103] T. Stepanenko, G. Zając, A. Czajkowski et al., "Sulfhemoglobin under the spotlight detection and characterization of SHb and $HbFe^{III}$-SH," *Biochimica et Biophysica Acta (BBA) Molecular Cell Research*, vol. 1870, no. 1, Article ID 119378, 2023.

[104] F. J. Romero, I. Ordonez, A. Arduini, and E. Cadenas, "The reactivity of thiols and disulfides with different redox states of myoglobin. Redox and addition reactions and formation of thiyl radical intermediates," *Journal of Biological Chemistry*, vol. 267, no. 3, pp. 1680–1688, 1992.